2018

Flow Visualization of R134a, R1234ze(E), and R1234yf in microchannel tube

Houpei Li
ACRC, the University of Illinois, hli84@illinois.edu

Predrag S. Hrnjak
pega@illinois.edu

Flow Visualization of R134a, R1234ze(E), and R1234yf in microchannel tube

Houpei LI[1], Pega HRNJAK[12*]

[1] ACRC, University of Illinois,
Urbana, Illinois, USA
hli84@illinois.edu

[2]Creative Thermal Solutions, Inc.,
Urbana, Illinois, USA
pega@illinois.edu

* Corresponding Author

ABSTRACT

This paper presents visualization results of two-phase flow of R134a, R1234yf, and R1234ze(E) in microchannel tube with hydraulic diameter of 0.643 mm. Visualization section has been made to record the flow in the microchannel to study the flow characteristic. Flow pattern maps of R134a, R1234ze(E), R1234yf are reported in this paper. Flow pattern maps are presented in two ways: mass flux-quality as coordinates, and superficial velocities as coordinates. The quality range of experiment is from 0 to 1 thermally. Mass flux varies from 50 to 250 $kgm^{-2}s^{-1}$. Flow patterns are classified as: plug/slug flow, transitional flow, and annular flow. The quality of boundary between two flow patterns is lower when mass flux is higher. At low vapor superficial velocity, the flow is in plug/slug. The vapor fraction and the interface velocity in plug/slug flow agrees well to the homogeneous prediction. As the vapor velocity increases, the flow becomes transitional flow. At higher vapor velocity and high liquid-to-vapor velocity ratio, the flow becomes annular.

1. INTRODUCTION

A new type of experimental facility for evaluation of heat transfer and hydraulic behavior in microchannel used in this work has been firstly introduced in Li and Hrnjak (2017). Heat transfer coefficients and pressure drops can be measured in one pass simultaneously in the six test sections. To further study the two-phase flow in microchannel tube, six visualization sections have been added after each test section on the facility.

Flow visualization could be tested on this facility and the liquid-vapor quality is controlled by adding or removing heat to the refrigerant. Another way to generate two-phase flow is mix two phase fluids such as Nino et al. (2002) who mix liquid and vapor phase R134a and Triplett et al. (1999) who mix water and air.

Table 1. Comparison of R1234ze(E), R134a, and R1234yf of physical properties at saturation temperature of 30 °C.

Property	Unit	R1234ze(E)	R134a	R1234yf
P_{sat}	kPa	578.4	770.2	783.5
P_R	-	0.159	0.190	0.231
σ	mN m^{-1}	8.21	7.42	5.56
H_{lv}	kJ kg^{-1}	162.9	173.1	141.2
ρ_l	kg m^{-3}	1146	1187	1073
ρ_v	kg m^{-3}	30.56	37.54	43.73
μ_l	kg $m^{-1}s^{-1}$ $\times 10^{-4}$	1.880	1.831	1.465
μ_v	kg $m^{-1}s^{-1}$ $\times 10^{-4}$	0.1246	0.1191	0.1255
ρ_l/ρ_v	-	37.5	31.6	24.5
μ_l/μ_v	-	15.1	15.4	11.7

R134a and R1234yf has similar pressure at the same saturation temperature of 30 ºC. However, they have different reduced pressure, thus different properties. R134a and R1234ze(E) have different reduced pressure and properties. However, HFOs (R1234ze(E) and R1234yf) has much smaller global warming potential than HFC (R134a). According to the 5th IPCC (2014), R134a has a GWP_{100} of 1300, R1234yf has a GWP_{100} of 4.0, and R1234ze(E) has a GWP_{100} less than 1. Table 1 provided some physical properties of the three refrigerants.

2. FACILITY AND DATA REDUCTION

2.1 Overview of Facility

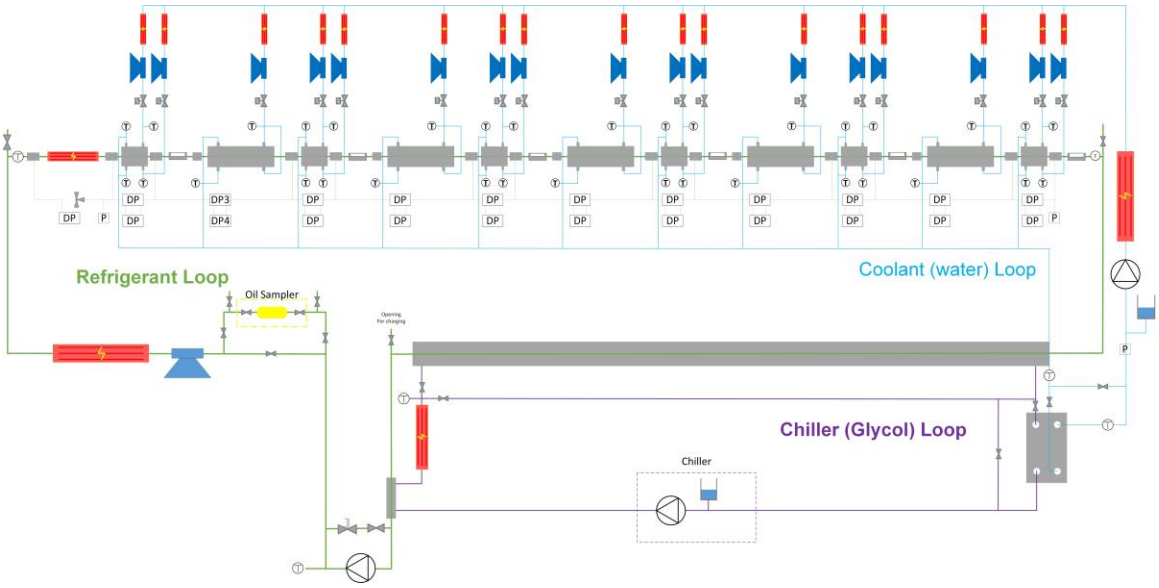

Figure 1. Schematic of the facility with refrigerant loop (green), coolant loop (blue), and chiller loop (purple).

The experimental facility has been introduced in Li and Hrnjak (2016) to study heat transfer and hydraulic behavior of refrigerants in microchannel tubes. The facility can measure heat transfer coefficient for a given heat flux, mass flux, and wall temperature. In the meantime, diabatic pressure drop and flow regime at exit of each test section can be collected. Adiabatic pressure drop can be measured separately without heat load. The facility is made of 3 loops: refrigerant loop, coolant loop, and chiller loop, as shown in Figure 1.

The detailed introduction of the facility can be found in Li and Hrnjak (2017) and Li (2016). A detailed schematic can be found in Li and Hrnjak (2018), as well as an experimental study of heat transfer coefficient and pressure drop of R1234ze(E) and R1234yf.

2.2 Visualization Section

As Figure 2 shows, the visualization section consists of an aluminum housing, a polycarbonate window, a steel frame, two aluminum flanges, a microchannel tube with top-wall removed, three O-Rings, and multiple bolts. The top wall of the tube in the visualization section has been removed by EDM. That created a 30-mm-long window in the center of the 152.4 mm long tube. The microchannel is machined carefully to make sure that only the top wall is removed. The T-shape polycarbonate window replaces the top wall, and the refrigerant is sealed by an O-ring made of Buna. The window only reaches to the position of top inner wall of microchannel tube when inserted into the house to make sure it doesn't interrupt the flow. Ten bolts fix the frame and window over the top flange to the house and press the O-ring. On the left and right sides, aluminum flanges and Buna O-Rings seal the refrigerant. During recording, a high-speed camera (Phantom V9.1) is fixed above the top of the section to the separate stand and takes video from there. An 1100 lumen LED flashlight provides needed light yet w/o significant heat input.

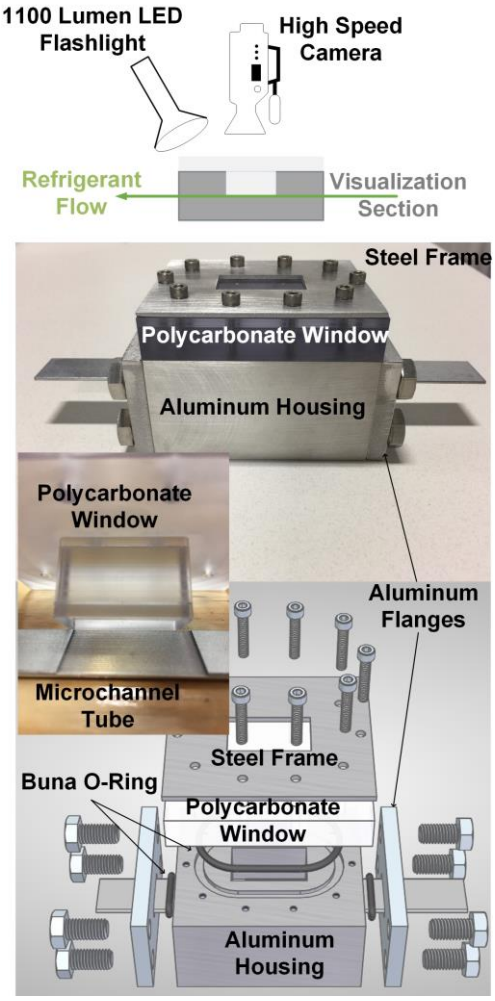

Figure 2. The visualization section contains a steel frame, a polycarbonate window, an aluminum housing, a microchannel tube with top wall removed, two aluminum flanges and three O-Rings

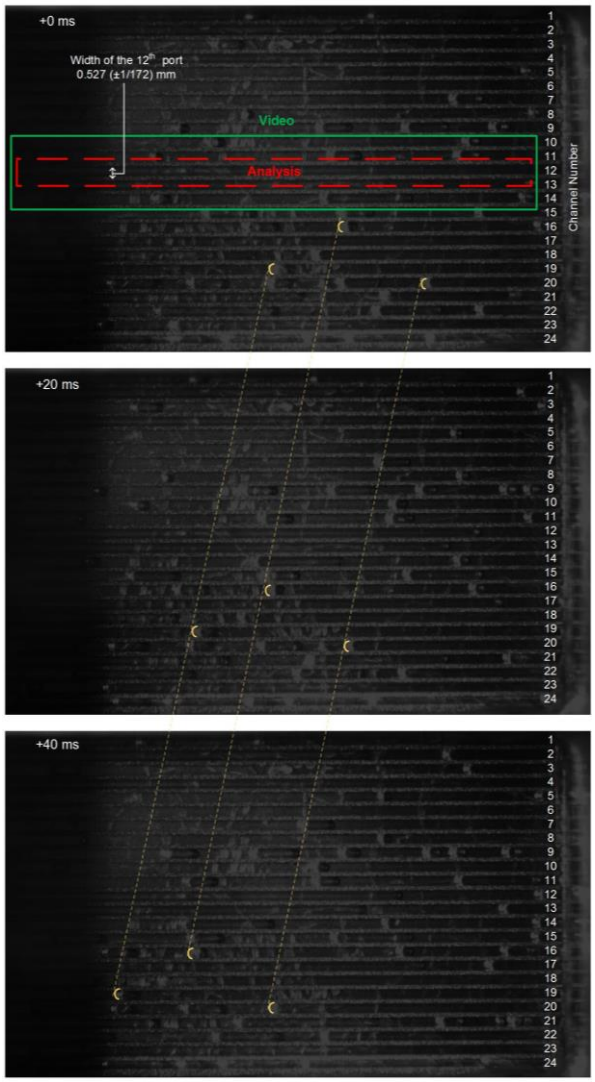

Figure 3. Captures of video at x=0.01, G=50 kg-m^{-2}s^{-1}. Green box is the position for video taking, red box is the position for flow analysis.

During each experiment, videos are taken at each one of six visualization sections with the same camera. The first video is taken at the visualization section 6 (Vs6) which has the highest vapor quality, and then Vs5, Vs4, to Vs1. The benefit of the video taking order is to further reduce the effect of heat input when section is exposed to the ambient or LED light.

An off-line test has been done to understand the heat effect of LED flashlight. The visualization section is made as Figure 2 shows except the microchannel tube is replaced by a T-type thermocouple. The temperature increases 0.61 ^{o}C in 10 seconds, 1 ^{o}C in 20 seconds, and 1.2 ^{o}C in 30 seconds. The rise stays at 1.4 ^{o}C after 1 minute. The video length varies from 2 to 10 seconds. So, the effect from flashlight appears to be insignificant.

2.3 Video Processing

There are 24 channels in the microchannel tube. Initial check indicated that regimes in all of them are identical. Further videos are taken only for 2-3 channels in the center of the tube, and the analysis is made for the same position (the 12th channel from top) at each of the six visualization sections, (see Figure 3). Due to the limitation of camera memory, when mass flux or quality is high, the video frame size needs to be reduced. As frame size is smaller, frame rate can

be larger in order to have a clear observation of the two-phase flow. The flow patterns are similar in all channels observed. Sometimes flow patterns are mixed and the definition of flow pattern is in subsection 3.1.

In plug/slug flow pattern, the interface of liquid-vapor is clear enough for tracking. The velocity of interface between vapor plug and liquid slug is calculated based on the position of interface of vapor plug and liquid slug. In different frames, the position (pixel) of the interface is tracked, as Figure 3 shows. The relation of number of pixels to length is based on the channel width. In the figure, the 12th port has a width of 0.527 mm. Tube channel size is measured by Mitutoyo WF microscope, and it has a resolution of 172 pixels in 1 mm. After the interface is located at multiple frames, a linear equation is fitted based on location and time. The slope of the equation is the velocity.

The vapor plug length is measured as Figure 4 shows. Firstly, the first pixel to the last pixel of one vapor plug is measured from video. The relation between pixel to length is calculated based on channel width. When vapor plug is longer than the frame size, frame rate are used in the calculation of velocity. For example, when the head of vapor plug appears at frame **a** and tail appears at frame **b**. If the frame rate is fps, and the velocity of the vapor plug is V. At the same position in frames a and b, the length pass is V(b-a)/fps.

The total length of vapor plug is corrected assuming that the plug head and tail are perfect hemisphere. The corrected length is used as the vapor plug length. The vapor plug fraction is vapor plug length divided by the total length of the video. When assuming the liquid film is insignificant to the total liquid volume in the channel, the vapor plug fraction is the void fraction.

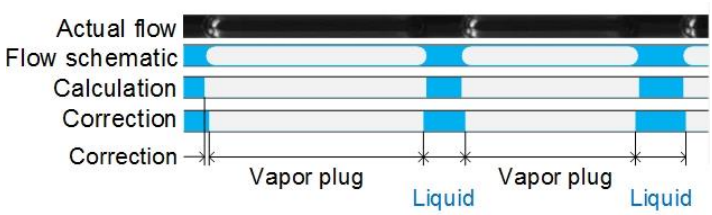

Figure 4. Illustration of the measurement of plug length in the plug/slug flow. The ratio of plug length to total length equals to void fraction if liquid film is ignored and the head and tail are hemisphere.

2.4 Error Propagation

Based on NIST technical Note 1297, the overall uncertainty (εR) of a result (R) with a known function F of n variables x_i with known uncertainties (εx_i) could be expressed in equation 1 (Taylor and Kuyatt, 1994). This equation is under assumptions that all variables are independent, repeated measurements show Gaussian distribution, and all uncertainties of variables are in the same level of confidence. In this paper, the level of confidence is 95%.

$$\varepsilon R = \sqrt{\sum_{i=1}^{n} \left(\frac{\partial F}{\partial x_i} \varepsilon x_i \right)^2} \tag{1}$$

Table 2. Uncertainties of instruments.

εP	1.25 kPa
εDP	0.0015 to 0.04 kPa
εT	0.07 to 0.2 °C
εm	0.1% to 0.15% of rate
ερ	0.0005 g-cm^{-3}

Instruments are calibrated to make sure the accuracy of measurements. The overall uncertainties of instruments are listed in Table 3. Ambient heat loss is measured and heat transfer rate is corrected. The contact resistance between heat transfer block to the microchannel tube is measured and the value is 0.0086 K W^{-1}. Tube channel size is measured by Mitutoyo WF microscope. The average diameter is 0.643 mm, and the standard deviation of diameters is 0.0232 mm. Detailed calibration process can be found in previous study (Li and Hrnjak, 2017) and the thesis (Li, 2016).

In this paper, flow pattern map will be presented as a function of mass flux and vapor quality, and as a function of superficial velocities. Mass flow rate is measured by mass flow meter and the flow cross-sectional area is measured by microscope. Vapor quality is determined by enthalpy. The inlet enthalpy (h_{in}) of test line is determined by pressure

and temperature measurements. Enthalpy of each test section is determined by adding or removing energy as equation 2 shows.

$$x_i = \frac{h_{in} + \frac{\sum_{n=1}^{i} Q}{\dot{m}} - h_l}{h_{fg}} \tag{2}$$

Flow pattern map is also presented based on superficial velocity. Superficial velocities of liquid and vapor phases are determined from equations 3 and 4.

$$J_l = \frac{G(1-x)}{\rho_l} \tag{3}$$

$$J_v = \frac{Gx}{\rho_v} \tag{4}$$

3. FLOW PATTERN MAPS FOR VARIOUS REFRIGERANTS

3.1 Classification of flow pattern

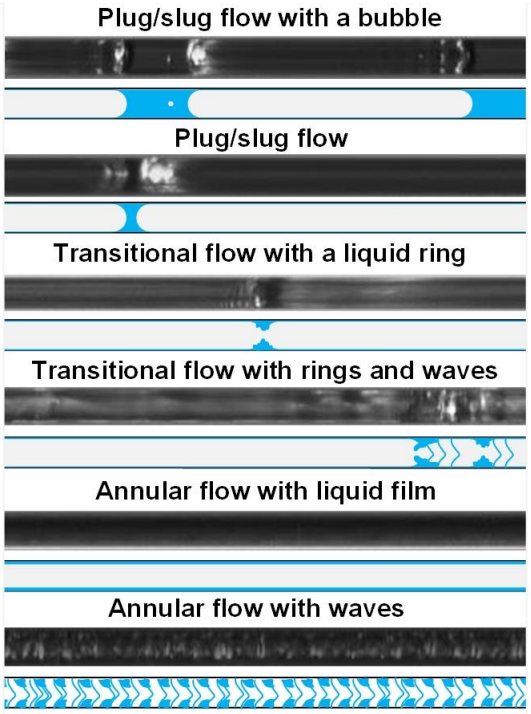

Figure 5. Flow patterns observation and classified as: plug/slug flow, transitional flow, and annular flow.

Figure 5 shows the flow patterns observed in the flow visualization videos. Three patterns are classified as: plug/slug flow, transitional flow, and annular flow.

The plug/slug flow is like the bubbly flow, intermittent flow, or slug flow in the literature. In this study, no observation shows a purely dispersed or bubbly flow. We always observe confined bubble in the video (First two captures in Figure 5). In plug/slug flow, a clear vapor plug can be observed from the video. In-between two clear vapor boundaries, it is the liquid slug. Sometimes bubbles can be observed at low quality or even thermally subcooling region. At high vapor quality but low mass flux, liquid slug is still in the tube and the vapor plug is can be very long. A significant characteristic of this flow pattern is that the flow is homogeneous. Vapor plugs and liquid slugs are moving at the same velocity. Velocity of liquid film is unknown due to limit of visualization technique, but it is predictable that the film has smaller velocity than the vapor plug.

In the transitional flow, vapor plug head and tail are not clear. This flow pattern is a transition from plug/slug flow to annular flow. This is similar to the churning flow, liquid-ring flow, or slug-annular flow in literature. A darker region can be observed in-between the blurry boundary of vapor plugs and it is a liquid ring with vapor bridge at center (the 3rd captures in Figure 5). At higher quality or mass flux, we see waves and droplets in the vapor zone, makes it similar to churning flow in literature.

In the annular flow, we see liquid film in the channel and at the center must be a vapor core when mass flux is lower and quality is higher (5th capture in Figure 5). Liquid film with waves is observed at higher mass fluxes (6th capture in Figure 5).

We believe that the transitional flow pattern is a transition for plug/slug flow to annular flow. Plug/slug flow occurs at lower quality. Annular flow occurs at higher quality. Transitional flow occurs between the plug/slug and annular flows. This shows that: as quality increases, the flow inertia breaks liquid slug and finally form a film. Sometimes the inertia is not enough to break all liquid slug so that liquid slug is always observable at all quality.

Sometimes two flow patterns occur at the same time. In some video, liquid slug and liquid ring are both observed in the same channel. In plug/slug flow, it can be defined as annular flow when one vapor plug is 700 mm long. Discussion of the long vapor plug is in subsection 4.3. The boundary between plug/slug to transitional flow is when the first liquid ring is observed. The boundary of annular flow is no liquid ring or liquid slug is observed in the video.

Flow pattern maps are reported in two coordinate sets. Mass flux and vapor quality is used as one of the coordinate sets and this is a common way to show the flow pattern map in the saturation dome. Another coordinate set is superficial velocities which is commonly used in literature especially in those studies with mix flow method for generating two-phase flow.

3.2 Flow pattern map of R134a

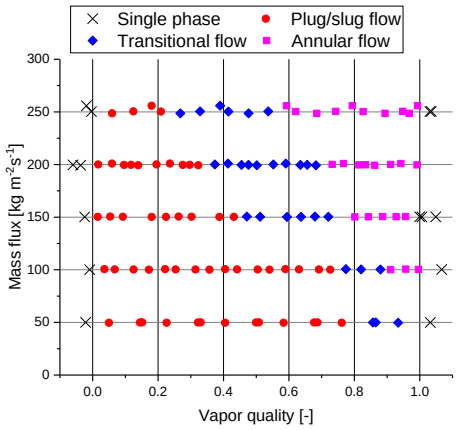

Figure 6. Flow pattern map of R134a at inlet saturation temperature of 30 ºC as a function of mass flux and quality.

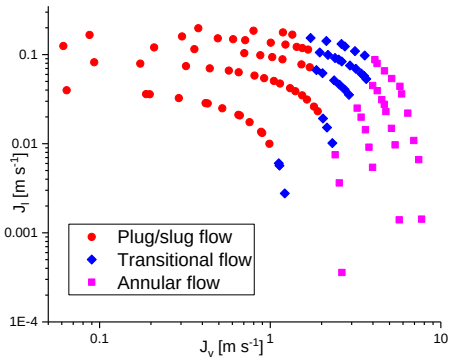

Figure 7. Flow pattern map of R134a at inlet saturation temperature of 30 ºC as a function of superficial velocities.

Figures 6 and 7 show the flow pattern map for R134a at inlet saturation temperature of 30 ºC. No annular flow was observed at mass flux of 50 kg-m^{-2}s^{-1}. As mass flux increases from 100 to 250 kg-m^{-2}s^{-1}, the quality of first observation of annular flow decreases from 0.9 to 0.6. The quality of the last observation of plug/slug flow decreases from 0.8 to 0.25 as mass flux increases from 50 to 250 kg-m^{-2}s^{-1}. The transitional flow always connects the plug/slug flow and annular flow when annular flow occurs.

In Figure 7, the flow pattern map is remade based on superficial velocities calculated from equations 3 and 4. Several quarter-circle curves from bottom to top in Figure 7 is a constant mass flux curve from 50 to 250 kg-m^{-2}s^{-1}. When the vapor superficial velocity is lower than about 2 m-s^{-1}, the flow is always in plug/slug flow. As the vapor velocity is higher than 1, the flow starts to become transitional. The vapor plug starts to break the liquid slug and connect to another plug as its velocity increases. As the liquid slug is broken, clear vapor plug boundary cannot be found in videos. As the vapor superficial velocity is higher and the liquid superficial velocity is lower, the liquid ring turn into

film and the flow becomes annular. The high vapor velocity will flatten a thick liquid ring. The high vapor to liquid slip ratio will cause waves in the flow.

3.3 Flow pattern map of R1234ze(E)

Figures 8 and 9show the flow pattern map of R1234ze(E). R134a and R1234ze(E) have similar flow pattern map because they have similar liquid and vapor properties according to table 1. At mass flux of 50 kg-m^{-2}s^{-1}, plug/slug flow ends at quality of 0.8 and becomes transitional flow. Annular flow is not observed at mass flux of 50 kg-m^{-2}s^{-1}. At mass flux of 100 kg-m^{-2}s^{-1}, annular flow occurs at quality of 0.85. As quality increases, qualities of first observation of transitional flow and annular flow decreases. In Figure 9, the vapor velocity of boundary between transitional flow and plug/slug flow increases as mass flux increases. The same trend could be concluded for boundary between annular flow and transitional flow.

3.4 Flow Pattern Map of R1234yf

Figures 10 and 11 show the flow pattern map of R1234yf. Flow pattern map of R1234yf is slightly different to R134a and R1234ze(E) due to the difference in properties in liquid and vapor phase. At mass flux of 50 kg-m^{-2}s^{-1}, plug/slug flow ends at quality of 0.95, and then transitioning to annular flow. No observation of transitional flow at mass flux of 50 kg-m^{-2}s^{-1}. As quality increases, quality of the first observation of transitional flow and annular flow decreases. Flow turns into transitional flow when the vapor superficial velocity is higher than 1 at mass flux of 50 kg-m^{-2}s^{-1}, and 2 ms^{-1} at mass flux is 250 kg-m^{-2}s^{-1}. Flow transitions to annular flow when vapor velocity is higher than 1.8 at mass flux of 50 kg-m^{-2}s^{-1}, and 4 ms^{-1} at mass flux of 250 kg-m^{-2}s^{-1}. The boundary between two flow patterns is a function of vapor-to-liquid-velocity-ratio.

3.5 Comparison of Three Refrigerants

Figure 12 shows the comparison of R1234yf, R134a, and R1234ze(E) at three mass flux, T_{sat} fixed at 30 °C. Overall, the three refrigerants have similar flow pattern maps at the same saturation temperature of 30 °C. Slight difference are found when comparing the three fluids at the same mass flux. When mass flux is 50 kg-m^{-2}s^{-1}, R1234yf is in annular when quality is higher than 0.95. Annular flow is not overserved at this mass flux for R134a and R1234ze(E). However, R134a and R1234ze(E) are in transitional flow when quality is higher than 0.8. At mass flux of 100 and 200 kg-m^{-2}s^{-1}, R1234yf always enters next flow pattern at higher quality than the other two refrigerants. R1234ze(E) enters the next flow pattern at slightly lower quality than R134a. Several properties contribute to the flow pattern maps. R1234yf has the highest reduced pressure among the three refrigerant, R134a is in medium, and R1234ze(E) is the lowest. The reduced pressure directly affects the surface tension and vapor density of refrigerants. R1234yf has much lower liquid viscosity than the other two refrigerants. Further research on analyzing the relationship between boundary of two flow patterns and physical properties can help a better understanding.

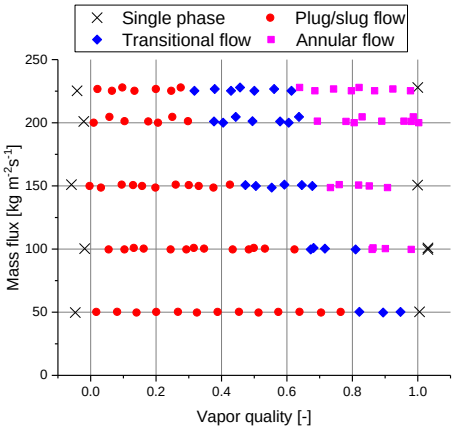

Figure 8. Flow pattern map of R1234ze(E) at inlet saturation temperature of 30 °C as a function of mass flux and quality.

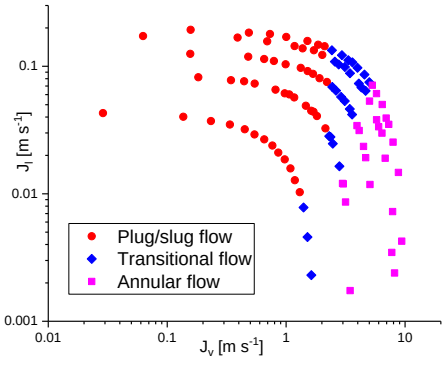

Figure 9. Flow pattern map of R1234ze(E) at inlet saturation temperature of 30 °C as a function of superficial velocities.

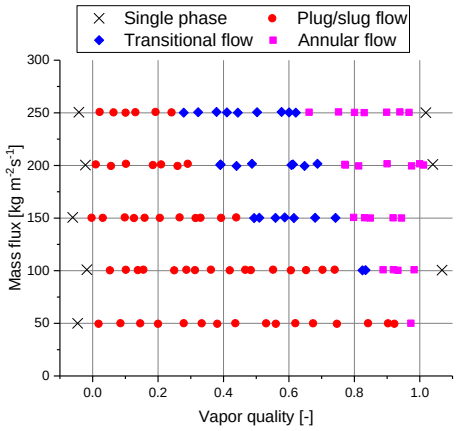

Figure 10. Flow pattern map of R1234yf at inlet saturation temperature of 30 ºC as a function of mass flux and quality.

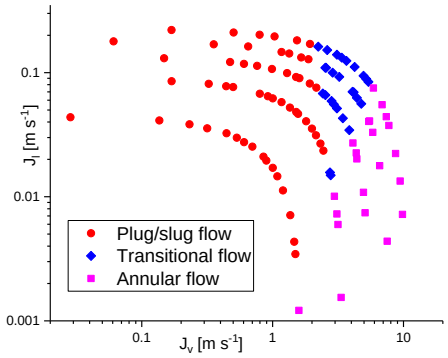

Figure 11. Flow pattern map of R1234yf at inlet saturation temperature of 30 ºC as a function of superficial velocities.

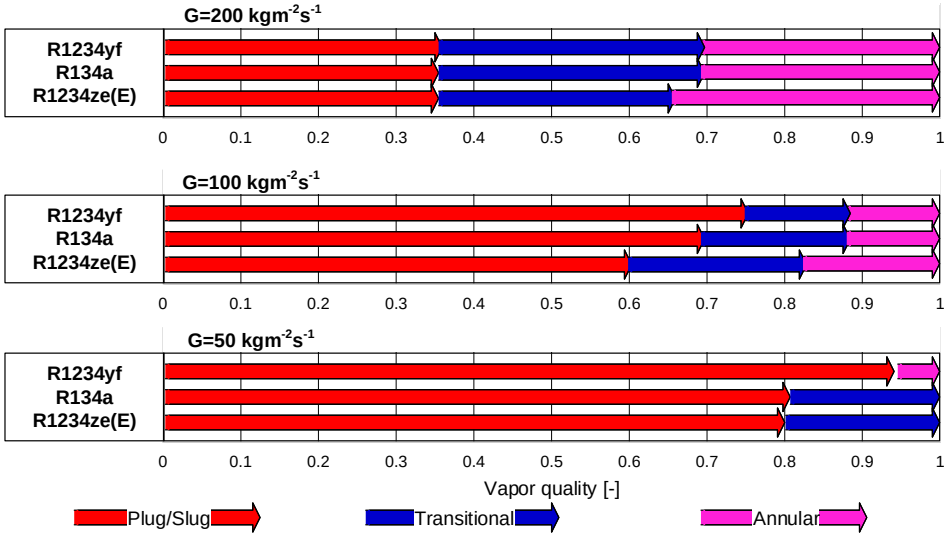

Figure 11. Comparison of R1234yf, R134a, and R1234ze(E) at three mass fluxes

3.6 Homogeneity of plug/slug flow in microchannel tube

Homogeneous velocity of two-phase flow is calculated based on homogeneous density and defined in equation 5. Noted that the homogeneous velocity is also the sum of liquid and vapor superficial velocities. The void fraction based on homogeneous assumption is defined in equation 6. In this paper, the interface velocity of plug/slug flow and the length fraction of vapor plug in plug/slug flow of R134a and R1234ze(E) are measured and compared to homogeneous model.

$$U_{tp} = G\left[\frac{1}{\rho_l} + x\left(\frac{1}{\rho_v} - \frac{1}{\rho_l}\right)\right] = J_v + J_l \tag{5}$$

$$\alpha = \frac{1}{1 + \frac{1-x}{x}\frac{\rho_v}{\rho_l}} \tag{6}$$

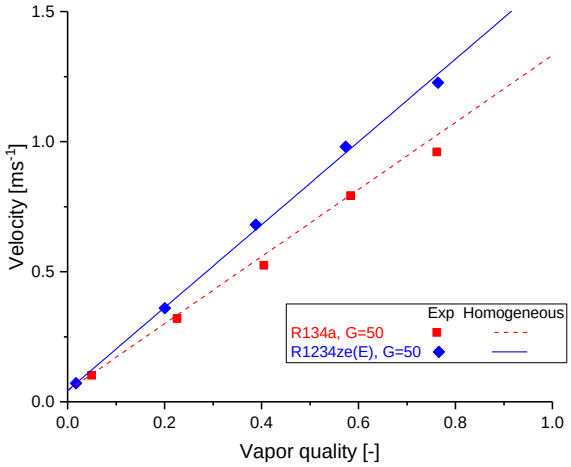

Figure 12. The interface velocity in plug/slug flow can be predicted by homogeneous velocity.

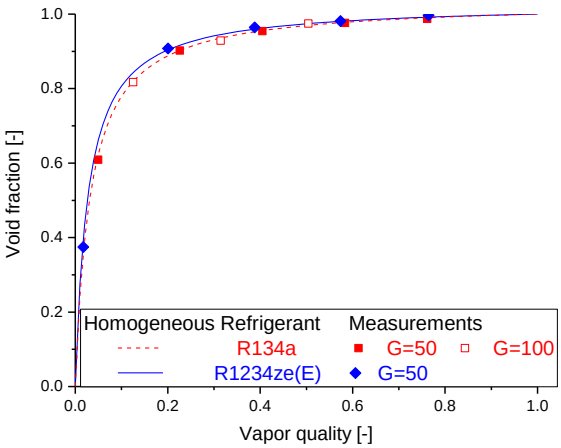

Figure 13. Vapor plug length fraction in plug/slug flow (represented by points) agrees to homogeneous model.

In Figure 12, velocity of vapor plug (vapor-liquid interface) in plug/slug flow of three refrigerants agrees to calculation from equation 5. The vapor plug and liquid slug are moving at the same velocity in plug/slug flow. The homogeneous assumption is hold in this case when the velocity of liquid film and the circulation velocity of liquid slug is ignored. Figure 13 shows that the vapor plug length fraction, which is close to the void fraction if volume of liquid film is insignificant. The measurements of R134a and R1234ze(E) at mass fluxes of 50 and 100 kg-m^{-2}s^{-1} show that the result agrees to homogeneous void fraction. Figures 12 and 13 show homogeneity of two-phase flow in plug/slug flow pattern. This measurement is helpful for building models for plug/slug flow pattern.

4. SUMMARY AND FUTURE WORK

A facility for visualization study in microchannel tube has been built and introduced. The flow pattern maps of R134a, R1234ze(E), and R1234yf are presented in this paper.

R134a and R1234ze(E) have similar flow pattern map due to similar physical properties according to Table 1. R1234yf has slightly different flow pattern map than the other two refrigerants as Figure 11 shows. Flow patterns are classified as: plug/slug flow, transitional flow, and annular flow concluded in Figure 5. The quality of boundary between two flow patterns is lower when mass flux is higher. At low vapor superficial velocity, the flow is in plug/slug. The vapor fraction and the interface velocity in plug/slug flow agrees well to the homogeneous prediction. As the vapor velocity increases, the flow becomes transitional flow. At higher vapor velocity and high liquid-to-vapor velocity ratio, the flow becomes annular.

Further research on expanding conditions and refrigerants is ongoing. Upcoming publications will present heat transfer coefficient, pressure drop, and flow characteristics of new refrigerants. Blends with low GWP refrigerant or oil mixtures will be included in the future. Condensation experiments will also be conducted on this facility.

NOMENCLATURE

D	Diameter	m
G	Mass flux	kg-m^{-2}s^{-1}
GWP_{100}	100-year direct global warming potential	-
H	Enthalpy	kJ kg-1
J	Superficial velocity	m-s^{-1}
P	Pressure	kPa
P_R	Reduced pressure	-
T	Temperature	K
x	Vapor quality	-

Greek leters		
ε	Uncertainty	-
μ	dynamic viscosity	Pa-s
ρ	density	kg m-3
σ	surface tension	N m-1

Subscripts

l	Liquid
lv	Liquid to vapor
v	Vapor

REFERENCES

IPCC, 2014: Climate Change 2014: Synthesis Report. (2014). Geneva, Switzerland: Contribution of Working Groups I, II and III to the Fifth Assessment Report of the Intergovernmental Panel on Climate Change [Core Writing Team, R.K. Pachauri and L.A. Meyer (eds.)].

Li, H. (2016). An Experimental Facility for Microchannel Research and Evaporating R134a in Microchannel Tube. University of Illinois.

Li, H., & Hrnjak, P. (2016). Heat Transfer and Pressure Drop during Evaporation of R134a in Microchannel Tubes. International Compressor Engineering, Refrigeration and Air Conditioning, and High Performance Buildings Conferences (pp. 1–10).

Li, H., & Hrnjak, P. (2017). Measurement of heat transfer coefficient and pressure drop during evaporation of R134a in new type facility with one pass flow through microchannel tube. International Journal of Heat and Mass Transfer, 115, 502–512. Elsevier Ltd.

Li, H., & Hrnjak, P. (2018). Heat transfer coefficient, pressure drop,and flow visualization of R1234ze(E), and R1234yf in microchannel tube. International Compressor Engineering, Refrigeration and Air Conditioning, and High Performance Buildings Conferences.

Nino, V. G., Hrnjak, P. S., & Newell, T. A. (2002). Characterization of Two-Phase Flow in Microchannels. Urbana, IL.

Taylor, B. N., & Kuyatt, C. E. (1994). Guidelines for Evaluating and Expressing the Uncertainty of NIST Measurement Results. Technology.

Nino, V. G., Hrnjak, P. S., & Newell, T. A. (2002). Characterization of Two-Phase Flow in Microchannels. Urbana, IL.

ACKNOWLEDGEMENT

This paper is a result of a project that was financially supported by the Air Conditioning and Refrigeration Center at the University of Illinois and its 30 member companies. CTS (Creative Thermal Solutions Inc.) provided complete technical support like material, instrumentation and previous 3 m long facility as a basis for the new, enlarged and improved facility used to acquire presented data. Authors also acknowledge support of Honeywell in providing the refrigerant R1234ze(E) and R1234yf.